

Article

Mechanical and Morphological Characterizations of Laminated Object Manufactured 3D Printed Biodegradable Poly(lactic)acid with Various Physical Configurations

Sudhir Kumar ^{1,*} , Inderjeet Singh ¹ , Dinesh Kumar ¹, Mohd Yazid Yahya ² and Seyed Saeid Rahimian Koloor ^{3,4,*} 

¹ Department of Mechanical Engineering, CT University, Ferozepur Rd, Sidhwan Khurd, Ludhiana 142024, Punjab, India

² Centre for Advanced Composite Materials, School of Mechanical Engineering, Faculty of Engineering, Universiti Teknologi Malaysia, Johor Bahru 81310, Johor, Malaysia

³ Institute for Nanomaterials, Advanced Technologies and Innovation, Technical University of Liberec, Studentská 2, 461 17 Liberec, Czech Republic

⁴ Institute for Structural Engineering, Department of Civil Engineering and Environmental Sciences, Universität der Bundeswehr München, Werner-Heisenberg-Weg 39, Neubiberg, 85579 Munich, Germany

* Correspondence: sudhirdwivedi1992@gmail.com (S.K.); seyed.rahimian@unibw.de (S.S.R.K.)

Abstract: Mechanical behavior of 3D-printed poly(lactic) acid material is an open topic for research on the reliability assessment of structures in marine and offshore industries. This article presents the mechanical and morphological properties of poly(lactic) acid specimens using the laminated object manufacturing technique. The effect was experimentally investigated on 3D-printed discs joined together to make a laminated test specimen. The specimen was prepared and tested under different infill patterns, viz. linear, triangular, and honeycomb structure, 50–90% infill density, and under varying disc thickness ranging from 3.4–5.6 mm. The maximum compressive strength of 42.47 MPa was attained for the laminated specimen with 70% infill, honeycomb pattern, and disc thickness of 3.4 mm (six discs), whereas the linear infill pattern has shown the least compressive performance of 22.40 MPa. The result of the study suggested that the honeycomb infill pattern with 90% infill density and six discs provides the optimum set of parameters for the 3D printing of PLA samples for maximization of compressive strength, especially for laminated object manufactured specimens. The Taguchi L9 orthogonal analysis (OA) suggested a significant influence on the infill pattern and the number of discs, contributing 51.60% and 48.29%, respectively, towards the compressive strength. Scanning Electron Microscopy (SEM) and toolmaker microscopic images have supported the observed experimental mechanical results for the laminated object manufactured specimens. The used technique of laminated object-manufactured components in the current study may have effective usage in marine and structural engineering fields.

Keywords: laminated object manufacturing; poly(lactic)acid; compressive strength; surface roughness; Taguchi analysis; 3D printing in marine application



Citation: Kumar, S.; Singh, I.; Kumar, D.; Yahya, M.Y.; Rahimian Koloor, S.S. Mechanical and Morphological Characterizations of Laminated Object Manufactured 3D Printed Biodegradable Poly(lactic)acid with Various Physical Configurations. *J. Mar. Sci. Eng.* **2022**, *10*, 1954. <https://doi.org/10.3390/jmse10121954>

Academic Editor: Vincenzo Crupi

Received: 26 October 2022

Accepted: 1 December 2022

Published: 8 December 2022

Publisher's Note: MDPI stays neutral with regard to jurisdictional claims in published maps and institutional affiliations.



Copyright: © 2022 by the authors. Licensee MDPI, Basel, Switzerland. This article is an open access article distributed under the terms and conditions of the Creative Commons Attribution (CC BY) license (<https://creativecommons.org/licenses/by/4.0/>).

1. Introduction

The marine industry gains an advantage from the design of complex parts and structures made of advanced polymeric materials [1–3] through new manufacturing technologies such as 3D printing, hot pressure die casting, injection molding, etc., [4,5]. Polymer composites have shown numerous applications in the design and manufacturing of components for structural and non-structural engineering [6–8]. To develop and characterize the polymeric properties on a lab scale, various modes of additive manufacturing (AM) technology, such as stereolithography, digital light processing, and fused deposition modeling, have been used extensively [9]. The selection of different polymeric materials is one of the critical steps in designing the experimental work, in which the material matrix plays a

vital role in deciding the application of the study [10,11]. There exist a range of polymeric matrices in the polymeric area that can be utilized depending on the usage and application of the research field [12,13]. Many polymeric matrices such as acrylonitrile butadiene styrene (ABS), nylon (NA6), polyvinyl chloride (PVC), polyethylene glycol (PEG), polyether ether ketone (PEEK), poly(lactic)acid (PLA), etc., have been used by different research groups [14–16]. These polymers can be used in a pure state or as a composite by using various reinforcements in the material matrix. PLA is one of such extensively studied materials which exhibits exceptional properties due to its biomedical compatibility and good mechanical characteristics.

Various research groups have studied the biodegradable properties of PLA due to its advanced mechanical and biomedical characteristics. One such study [17] has reported the flexibility of 3D printing of porous PLA structures for replacing injured tissues with the polymeric scaffold. The porous structure has led to a reduction in the degradation behavior of the scaffold by giving real-time fluidic conditions [17]. Sometimes, the mechanical properties, such as toughness, also get affected by the direction of fused polymer deposition on the 3D printing surface. It has been observed that the toughness got improved for the 3D printed specimen when tested in the same direction of polymer deposition. Furthermore, the annealing cycle up to glass transition temperature has shown an insignificant effect on the mechanical characteristics, while the strength of the specimen was found to be decreased drastically [18].

The PLA reinforced with calcium phosphate (CaP) glass particles has improved biomedical activity for tissue regeneration. The presence of CaP particles in the PLA matrix has improved the cell adhesion properties, due to which the biocompatibility of the PLA composite has increased. The flexibility of the FDM process has made the scaffold porous and interconnected, which enhanced the biomedical importance of the composite, especially for tissue regeneration [19]. The reinforcement of magnesium (Mg) in PLA up to 15 wt% has improved mechanical results for surface hardness and elastic modulus and a decrease in the flow index for the composite [20]. The 3D printing input parameters play a vital role in deciding the specimen's mechanical and morphological characteristics. An infill density of 100% has shown the maximum young modulus of the 1538 MPa for the PLA material matrix. In contrast, the 90 mm/s infill speed for 3D printing has the maximum effect on young's modulus compared to the similar behavior of 70 mm/s and 110 mm/s infill speed [21].

Pure PLA has been tested for tensile and compression properties according to the ASTM D695 standard. The tensile-tested specimen of pure PLA printed with a 45° orientation has shown a maximum tensile strength of 63 MPa. While in the case of compression testing, the maximum young's modulus has been observed to be 2053 MPa [21]. In one of the studies of pure PLA under compression testing, it has been observed that the printing parameters are of great importance. In that study, infill density, infill speed, and layer height were the main input parameters selected by the researcher. The study highlighted that the maximum compressive strength was observed for a maximum infill density of 80% among the tested infill densities of 60, 70, and 80%, along with the maximum layer height of 0.3 mm among the different input levels of 0.1, 0.2, and 0.3 mm [22]. One such study based on laminated object manufacturing (LOM) of polyvinyl chloride (PVC) reported the advantages of LOM by improving the aesthetic part of produced objects. The orientation of the layers manufactured on FDM printing also played a vital role in the selection of optimized specimens from the samples tested for mechanical properties [23].

Flax fiber reinforcement in PLA matrix, which may act as the biodegradable polymeric matrix, has been studied for compression properties. The study results highlighted that flax fiber had shown greater normalized residual strength compared to carbon/epoxy laminates. The failure mode suggested that the fiber failure occurred in flax fiber laminates of PLA. In the case of a non-biodegradable sample of PLA, delamination was the main reason for the composite failure [24]. Flax fiber reinforcement of 30 wt% has shown maximum tensile stress and modulus in comparison to pure PLA and PLA/tri-acetin/flax fiber composite.

The maximum tensile stress of 54 MPa and 8.3 GPa of young's modulus has been observed for the PLA/30 wt% flax fiber composite. However, the study highlighted there was hardly any effect of plasticizers on the properties of PLA material matrix composite [24]. A similar study on the LOM of PVC using different build orientations by Olivier et al. 2016 [25] has reported that the produced specimen was stronger for the direction in which the material was 3D printed on the FDM setup. The build orientation of 45° resulted in the maximum flexural strength of the LOM PVC specimen.

PLA in reinforcement with hydroxyapatite (HA) has been explored for manufacturing porous scaffold applications. The addition of the HA phase in the PLA matrix has led to an increased recovery stress value of 3 MPa at 70 °C. The HA has also improved the shape recovery of the PLA composite scaffold by 96% [26]. The infill pattern has also played a significant role in deciding the compressive strength of the PLA composite material matrix. One of the studies has reported that the infill pattern of the Hilbert curve with a maximum infill density of 80% has reported 122 MPa of compressive strength. At the same time, the rectilinear pattern of 3D printing has shown the least mechanical properties [27]. Tao et al. 2021 [28] worked on laser-cut veneer laminated object manufacturing (LcVL) through the additive manufacturing (AM) route. Different complex design has been printed and laminated using the top surface of polyvinyl acetate (PVA) as an adhesive. The study reported that the LcVL method was suitable for producing wood-based LOM parts with high efficiency.

A PLA/HA composite of up to 15 wt% has been studied, and it is reported that HA reinforcement in PLA has not resulted in the expected flexural modulus of the composite, due to which the composite has shown lower properties than human cortical bone [7]. Researchers have also observed the critical behavior of the PLA specimen for the buckling effect under compression loading. The slenderness ratio of the sample has been reported as the critical parameter for the buckling effect. The maximum compressive stress of 58 MPa has been observed for the specimen length of 65 mm. The buckling effect was evident in the slenderness ratio of 9.5 [29]. PLA in the reinforcement of chitosan has been explored up to the reinforcement level of 1, 1.5, and 2 wt%. The results have concluded that the 1.5 wt% reinforcement level of chitosan in the PLA matrix was the optimum reinforcement level. The optimized processing condition of 1.5 wt% loading of chitosan in the PLA matrix has resulted in a maximum tensile strength of 40 MPa, a compressive strength of 42 MPa, and a flexural strength of 118 MPa [30]. Wang et al. 2022 [31] have reported on the LOM manufacturing of gun propellants and compared the results with conventional double-based gun propellants. The results of the study highlighted that there was a comparable density between the LOM-based and conventional-based samples. The LOM-based sample resulted in a 35% improvement in the progressive combustion of gun propellants.

Some research studies have highlighted the use of PLA in the reinforcement of Fe₃O₄, wood powder, and Polyvinyl chloride (PVC) for 4D applications such as self-assembly of the material matrix. The reinforcement of Fe₃O₄ and wood powder in the PLA matrix has resulted in the superparamagnetic properties in the nonmagnetic PLA matrix [29,30,32]. Researchers have reinforced the matrix of PLA with four different raw materials, (a) plain jute, (b) basket cotton, (c) basket flax, and (d) plain flax, through a compression molding route and have tested the mechanical properties. The results have emphasized that the basketweave flax in the PLA matrix has a maximum effect on the mechanical properties of the PLA matrix by improving the tensile strength of PLA up to 116.33 MPa [24]. The infill percentage of 60% in the case of 3D printing has given maximum porosity among selected input infill percentages of 60, 70, and 80%, which was found to be effective for the biocompatibility of PLA-based scaffolds [33]. When explored for scaffold printing application, the almond skin-reinforced PLA matrix has resulted in compressive strength of 38 MPa for an infill density of 100% and infill speed of 70 mm/s [34]. Various other studies exist that have highlighted the properties of PLA for different mechanical properties by varying the reinforcement material, such as PLA/Copper (Cu) composites [35],

PLA/Collagen/Chitosan [36], PLA/Fe₃O₄/Wood powder [37] composites, and PLA/PEG composites [38] for biomedical applications such as scaffold printing.

Parandoush et al. 2021 [39] performed laser-assisted LOM manufacturing of continuous carbon fiber reinforced epoxy composite (CFREC) [16] in which interfacial layers contain graphene. The prepreg sheet was LOM manufactured, and the result suggested that when CFREC was LOM manufactured using graphene in interfacial layers resulted in low porosity values, improved bonding between the laminated layers, and improved mechanical properties. Pan et al. 2022 have established that sandwiched structure of polymeric material may have a vital role to play in sensor applications. The study has shown that TPU may be used as a flexible sensor when a carbon nanotube (CNT) is sandwiched between two layers of TPU. The sandwiched structure has shown some reduction in the tensile strength of the TPU but exhibited the required strength for sensor application that was sufficient for flexible sensor applications [37].

Han et al. 2021 worked on sandwiched structures of TPU and silver (Ag) particles for high-stretch sensor applications. From the study, it was observed that with the addition of an extra layer of Ag inside the TPU, the stress-absorbing capacity of the sandwiched structure increased, but the percentage elongation of the specimen decreased significantly [38]. Singh et al. 2019 prepared a sandwiched structure of PLA, HIPS, and ABS altering the position of materials. The results of the study suggested that with multi-material specimens, the properties of the newly developed structure lie in between the parent material properties but the functionality and application of the structure increase significantly [39].

Previous studies have reported the use of FDM printing of critical components for marine applications, such as components of specialized underwater vehicles or water surface vehicles, and the study of hydrodynamics and biomechanics using FDM-printed prototypes of polymeric materials [40]. One of the studies on PLA material characterization has successfully implemented FDM printing for hexagonal lattice structures, which could have tremendous application for marine and other structural engineering filed as the lattice structure provides improved mechanical properties [41]. The polymeric material PLA has been tested in computational flow dynamics conditions giving real-time fluidic conditions has revealed that there are chances of degradation with time due to the saline nature of ocean water and increasing surface roughness increased the rate of degradation [1,42].

One of the previous studies reported by Kumar et al. [43] suggested a modified way for using FDM printed parts as laminated parts to produce a single specimen and suggested improved compressive strength of the samples. Parandoush et al. [39] worked on a new technique of laser assisted-LOM of carbon fiber-reinforced sheets and used graphene as a reinforcement between laminated layers to improve the strength of the joined part. Several studies have taken design consideration for FDM printing and other technique, which have shown an impact on the characteristics of the material used in the study [44–48].

2. Scope for the Present Study

The extensive literature review revealed that different studies have worked on characterizing the PLA material matrices with various reinforcements. The common and most vital point among all the studies was the exploration of the mechanical behavior of pure PLA and reinforced particle matrix of PLA for improving the mechanical, morphological, thermal, and electrical properties, etc. But hitherto, little has been reported on the laminated object manufacturing (LOM) technique in the case of PLA material matrix by diving the single component into different layers and joining those layers with suitable adhesive for the characterization of mechanical and morphological properties. These laminated objects may have specific applications in the marine engineering field, such as in components of special-purpose marine vehicles or instruments working underneath the water.

The technique used for preparing the LOM object is not through the LOM printer; rather, a single specimen of 25.4 mm height was divided into several objects (4, 5, and 6) depending on the thickness of the discs, and then glued together using epoxy resins. This method of preparing LOM objects was selected because of the lenience of the technique

and because the FDM printed objects can be arranged to form LOM samples, which may have better results than normal FDM printed samples.

Significance of the Current Work

Different research studies have highlighted that pure PLA or composite of PLA reinforced with foreign particles have been used for various applications varying from engineering to biomedical applications. But no study dealt with the dissection of a single specimen into several parts and then bonding them with suitable techniques and exploring the mechanical and morphological behavior of such LOM specimen of single polymeric material, as investigated in this research. In addition, the current study guides future researchers to explore the LOM technique for 3D/FDM printed parts with better control of mechanical and morphological characteristics. The components developed by FDM may be joined as a single product using the suggested LOM-epoxy method. The developed components may have suitable applications in marine engineering as the components under ocean water have seen degradation with time. The degraded components can be replaced with new components as per requirements. The LOM technique used in this study may be used in applications where the exposed surface polymer gets degraded with time. The degraded portion can be cut off from the surface, and a new FDM printed specimen can be fixed to the sample using epoxy resins.

3. Materials and Method

3.1. Preparation of Test Specimen

In the present study, an effort has been made to study the effect of laminated object manufacturing of PLA by dividing the single component into many pieces while 3D printing and joining those 3D printed specimens into one specimen for standard testing. Following are the important aspects that have been selected for the study, which may have a vital role to play in the LOM manufacturing of PLA. There are many parameters of FDM that may be taken as variables, but this study is limited to 2 FDM parameters (a) infill density and (b) infill pattern, and one design parameter number of the disc to study the effect of lamination of discs with each other. The porosity level below 50% may affect the strength of the material, whereas previous literature has shown the positive impact of increasing the infill percentage on FDM printed parts. Therefore, the porosity level has been chosen from 50% and is varied to 90% to accommodate the effect of the infill pattern.

1. **Selection of material:** For this purpose, the spool of biocompatible PLA polymer has been purchased from the local market (Shiva Chemicals, Ludhiana). The PLA material for 3D printing has been chosen as the material matrix has wide application in biomedical applications, especially scaffold printing. Table 1 shows the PLA basic properties used for the current study;
2. **Design of experimentation:** Taguchi L9 orthogonal array (OA) has been used to design the experimentation work. Table 2 shows the design of experimentation (DOE) used for 3D printing. An open-source fused deposition modeling machine (FDM) has been used to 3D print the specimens. Cylindrical specimens 12.7×25.4 mm were 3D printed as per ASTM D790 standards. For FDM printing the PLA discs, some fixed and variable conditions of 3D printing were used. Table 2 shows the variable conditions of the FDM printer. Table 3 shows the fixed conditions of 3D FDM printing. The 3D-printed specimens were then joined using standard glue, which is used to join the wood or polymeric material. The single standard laminated sample held a different number of pieces in each specimen depending on the selected thickness of the 3D-printed workpiece. The standard sample was 25.4 mm in height the sample in which 4 discs were joined held a thickness of 5.6 mm. Figure 1 shows the (a) sliced images of 3D specimens, (b) real-time images of 3D printed specimens, (c) 3D printed 9 different discs, (d) single specimen with size specifications, and (e) number of upper- and lower-layer combinations for the study;

3. **Number of discs:** Table 4 shows that multiple discs were 3D printed, varying the thickness of discs ranging from 3.4, 4.28, and 5.6 mm. The standard sample for compression testing has a 12.7×25.4 mm standard cylindrical shape; therefore, in the present study, multiple discs were 3D printed and joined with each other to explore 3D printed specimens. For example, in the case of the disc with a thickness of 3.4 mm, 6 specimens were joined together using suitable adhesive with 1 mm adhesive layer thickness leading to a 25.4 mm total height of the sample. As per the fixed condition of FDM printing, 4 lower and upper solid layers were used in each disc (Figure 1e). In the case where there were 4 discs laminated in a single sample, there were a total 32 number of layers (4 upper and 4 lower layers in each disc \times 4 discs = 32 layers). Table 4 also shows the number of upper and lower layers in the FDM printed specimen in relation to the number of discs present in the single standard disc for compressive testing;
4. **Maintenance of the glue thickness between the layers:** To maintain the glue thickness between the layers, three cylindrical setups were prepared with 1 mm slots at the required places. The cylindrical discs were fitted inside the slot, and epoxy resin was filled to maintain the proper thickness of glue between the layers.

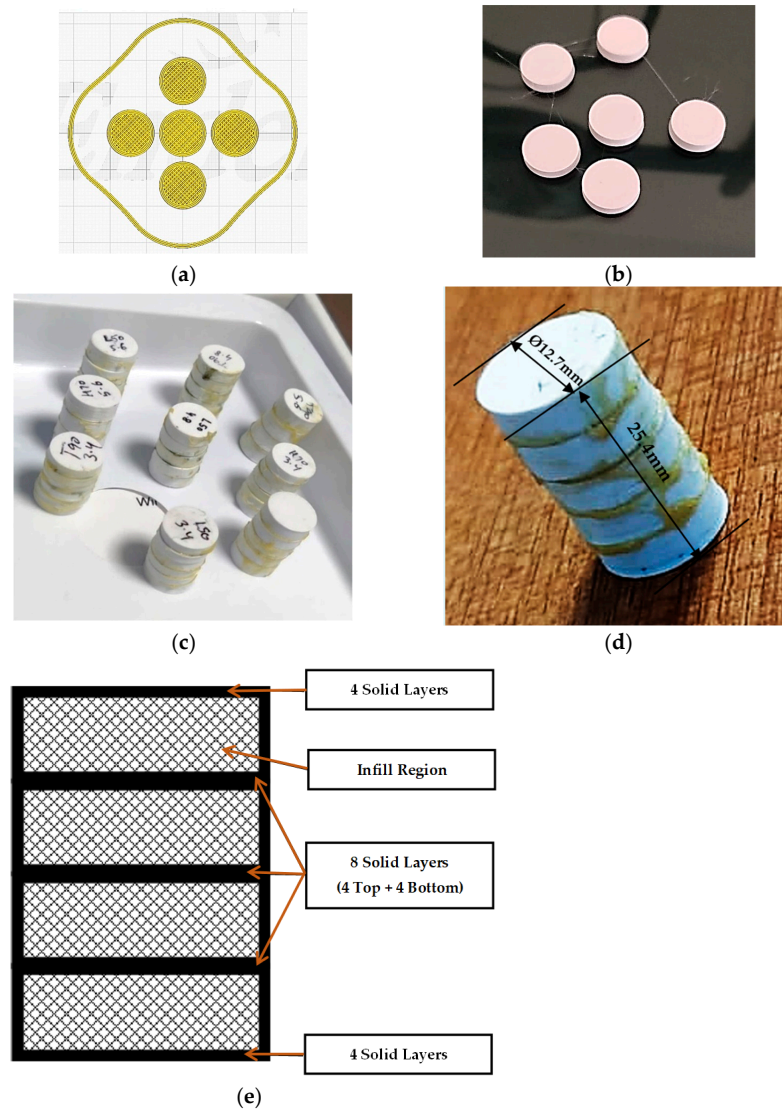


Figure 1. (a) 3D Sliced image, (b) real-time images of 3D printed specimens, (c) nine samples by joining multiple discs (standard size of 12.7×25.4 mm) as per DOE, (d) Single sample of PLA with dimensional detail, and (e) Schematic of solid and infill layers in the laminated specimen having 4 discs.

Table 1. Properties of PLA used in the current study according to the manufacturer.

Properties	Values
Tensile Strength	16–80 MPa
Modulus of elasticity	0.23–13.8 GPa
Glass transition Temperature	64–68 °C
FDM working Temperature	200–210 °C

Table 2. DOE using Taguchi L9 OA for LOM of PLA material matrix.

Sample No.	Infill Pattern	Infill Density (%Age)	Number of Disc
1	Linear	50	6
2	Linear	70	5
3	Linear	90	4
4	Triangular	50	5
5	Triangular	70	4
6	Triangular	90	6
7	Honeycomb	50	4
8	Honeycomb	70	6
9	Honeycomb	90	5

Table 3. Fixed condition used for FDM printing.

S.No.	Parameters	Values
1	Bed Temperature	60 °C
2	Fan power	50%
3	Nozzle Temperature	240 °C
5	Surface Fill	Line at 45°
6	FDM Printing speed	40 mm/s
7	Number of perimeters	3
8	Layer height	0.12 mm
9	Line Width	0.4 mm
10	Number of Upper Layers (Single disc)	4
11	Number of Lower layers (Single disc)	4

Table 4. Disc thickness for different numbers of discs and number of upper and lower layers.

S.No.	Single Disc Thickness (mm)	Number of Discs	Number of Upper and Lower Layers
1	3.4	6	48
2	4.28	5	40
3	5.6	4	32

3.2. Compression Testing for Prepared Samples and Methodology

The prepared samples were tested for compression properties using ASTM D695 standard conditions. The sample was tested with a speed of 30 mm/s. The machine used for compression testing was a universal tensile testing machine (UTM) with a suitable testing setup with subassembly on the UTM machine. Figure 2 shows the sample under

compression testing in a real-time environment. Figure 3 shows the (a) tested samples of PLA on the UTM for compressive strength and (b) sample 3 with the least mechanical performance, and (c) sample 8 with the maximum mechanical strength. Figure 4 shows the chosen methodology of the current work. To calculate the optimized compressive strength per the Taguchi analysis, the following calculations were made

$$\eta_{opt} = Z + Z_{A1} - Z + Z_{B1} - Z + Z_{C2} - Z \tag{1}$$

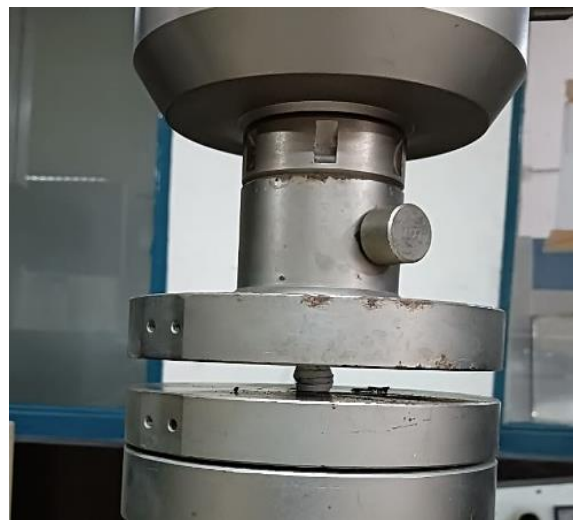


Figure 2. A sample under compression testing on the UTM machine.



(b)



(c)

Figure 3. (a) PLA samples tested on the UTM for compressive strength, (b) sample 3 with the least mechanical performance, and (c) sample 8 with the maximum mechanical strength.

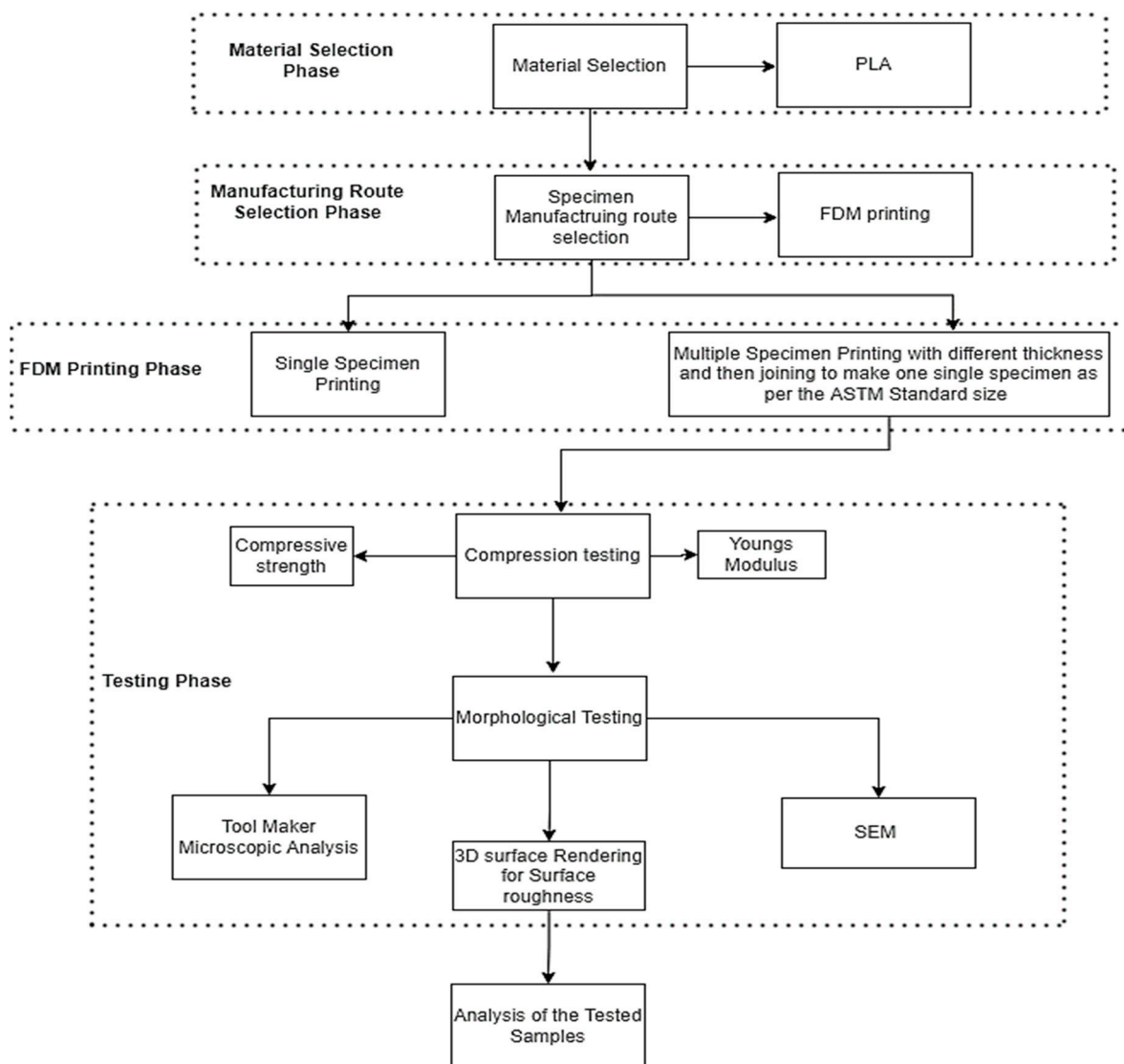


Figure 4. Our methodology for exploring the mechanical and morphological characteristics of 3D printed PLA.

3.3. Morphological Testing

The destructed/tested samples were cut from the mid-section and were tested for morphological characteristics using SEM and a toolmaker microscope.

To analyze the failure mode of the developed 3D printed part subjected to a compressive test, the fractured specimen was cut into 2 halves with a polymer cutter (Model: NGB814695; Make: NETZSCH, Selb, Germany), the outer curved surface of the specimen was examined under SEM (Model: EVO 18 Special Edition; Make: ZEISS Microscopy, Jena, Germany). Before SEM, the surface of the specimen was gold coated using fine coater (Model: JFC-1200; Make: JEOL, Ltd., Tokyo, Japan) to improve its conductivity. The photomicrographic image obtained from the SEM was further subjected to 3D rendering using open-source “Gwydion” software.

4. Results and Discussion

4.1. Mechanical Properties

The specimen prepared using the LOM technique for 3D printed samples of PLA has been tested for compressive properties using the UTM setup present at the Centre for Skilling and Technical Support (CSTS), Amritsar, India. The testing was performed at a

steady rate of 25 mm/s. Table 5 shows the compressive strength of the different samples tested on UTM. The result shows that the maximum compressive strength was observed for sample 8, prepared with a honeycomb infill pattern, an infill density of 70%, and a disc thickness of 3.4 mm (six discs). This sample behavior may be due to a low thickness value for the discs. The low-thickness disc may have reduced the internal stress of the component. The thickness of 3.4 mm for disc resulted in 6 discs combined in a single specimen.

The large number of discs combined into one sample may reduce the stress concentration of the samples. From the results in Table 5 (for samples 7 to 9), it may be observed that the honeycomb infill pattern has shown better compressive strength. The infill density has shown a moderate effect on the compressive strength of the sample. From Table 5, one can observe that the honeycomb, along with the infill density of 70%, has resulted in better strength than sample 9, which is also made from a honeycomb pattern but with an infill density of 90%. The least properties were observed for sample 3, which was 3D printed with a linear infill pattern, 90% infill density, and four discs. The smaller number of discs, along with the linear infill pattern, has resulted in poor mechanical performance, as can be seen from the test report of sample 3. From Figure 3b,c, one may observe that a sample with a smaller number of discs has resulted in more bulging of the sample due to the large thickness of the disc, whereas with the maximum number of discs has resulted in the least bulging thus performing better for compressive strength. This may be due to the reason that a large number of discs resulted in less thickness of each disc in a single specimen. In the case of the sample with 4 discs, more volume has partial infills with voids and voids and is therefore subjected to skewness. Whereas, when the disc is increasing, the volume with infills and voids decreases, resulting in less skewness.

Figure 5 compares compressive strength for different infill patterns with the number of discs used with the LOM technique. From Figure 5a, it may be observed that the increasing number of discs increased the strength of the component for linear patterns. Similar trends were observed for the triangular infill pattern, as shown in Figure 5b. From Figure 5c, the increasing number of discs in one specimen is favorable for PLA samples in the case of a honeycomb infill pattern.

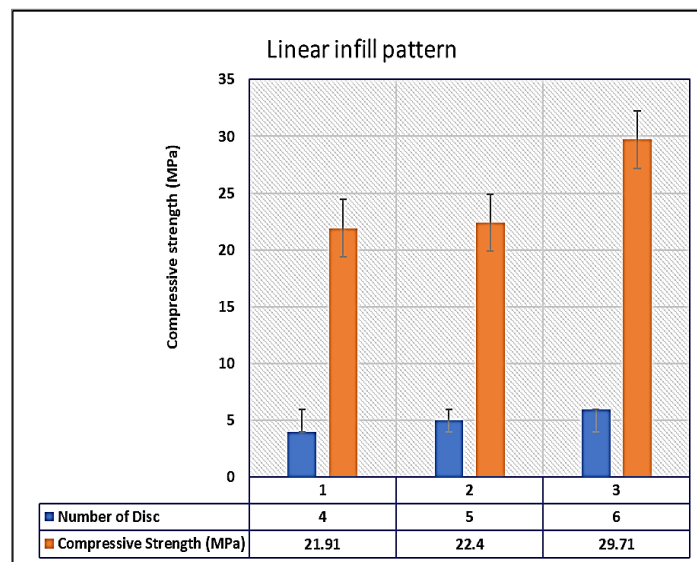
The maximum mechanical strength has been given by the honeycomb infill pattern (compressive strength: 42.47 MPa) with six discs (sample number 8) combined in a single sample compared to all other infill patterns. The triangular infill pattern has shown the second-best result (compressive strength of 36.06 MPa) after the honeycomb infill. A linear pattern with 4 discs in one sample (sample no. 3) has shown the least mechanical performance of 22.40 MPa.

The LOM-manufactured sample of single material has shown better results than the multi-material specimens tested by past researchers. Past research studies highlighted that there was a significant reduction in the mechanical properties of the specimen when the sandwich structure of different materials was prepared according to needs, such as sensor applications, highly flexible/stretchable sensors, and other applications [37–39]. The current work reports the improvement in the LOM-manufactured sample with a large number of dissections of a single specimen.

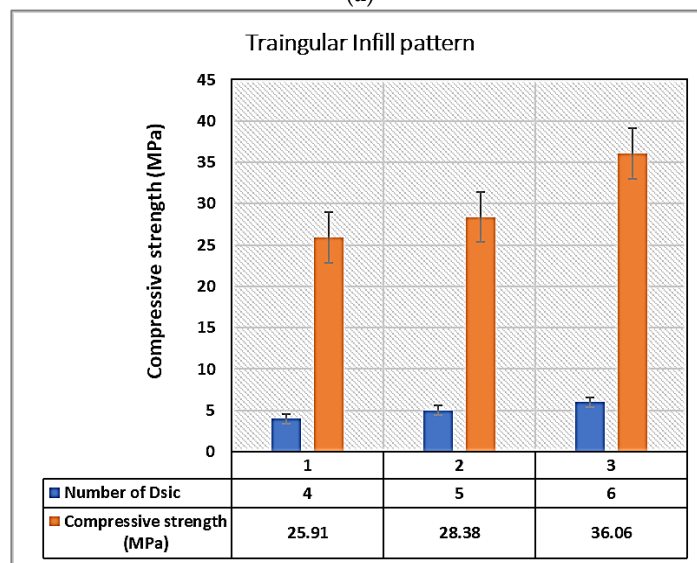
The results obtained for compressive strength were better than the FDM printed samples. The research report produced by Singh et al. [34] has obtained maximum compression strength of 37–38 MPa for Cu-reinforced PLA, whereas in the proposed methodology maximum strength obtained for virgin PLA was found to be 42.47 MPa. In contrast, the current study has reported better results than normal FDM printed compression sample PLA-Cu feedstock, but different studies have been found which report better as well as on-par results because the properties depend largely on FDM input variations such as infill pattern, infill percentage, number of layers, or their further combination with different reinforced material matrixes [49].

Table 5. Mechanical properties of LOM manufactured PLA samples.

Sample No.	Infill Pattern	Infill Density (%Age)	Number of Discs (mm)	Compressive Strength (MPa)
1	Linear	50	6	29.71
2	Linear	70	5	22.40
3	Linear	90	4	21.91
4	Triangular	50	5	28.38
5	Triangular	70	4	25.91
6	Triangular	90	6	36.06
7	Honeycomb	50	4	30.38
8	Honeycomb	70	6	42.47
9	Honeycomb	90	5	32.75



(a)



(b)

Figure 5. Cont.

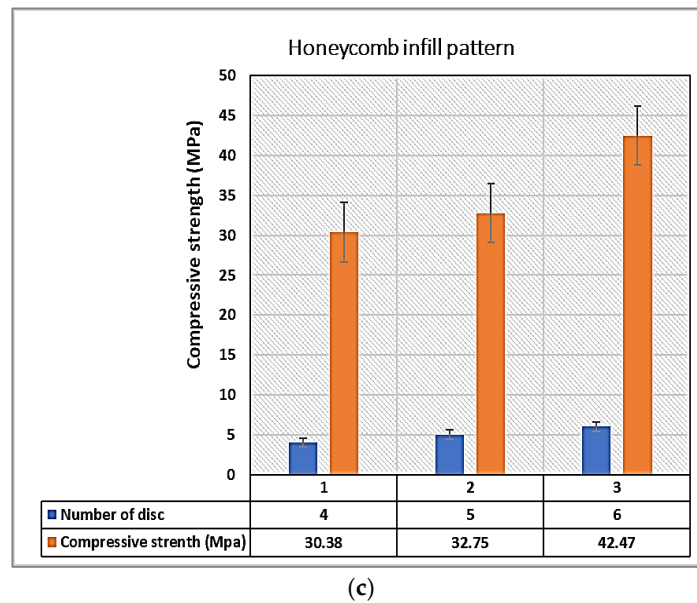


Figure 5. Comparison of mechanical strength with the number of discs with varying infill patterns for (a) linear, (b) triangular, and (c) honeycomb patterns.

4.2. Taguchi Analysis

The result obtained from the compressive testing were further analyzed to optimize the finest 3D printing setting by using Taguchi L9 OA-based analysis. From the study, different charts were obtained, such as signal-to-noise (SN) ratios, an Analysis of variance table for SN ratios, a Rank table for compressive strength values, and the main effect plot for the optimized settings of 3D printing. Table 6 shows the analysis of variance (ANOVA) for SN ratios using Taguchi analysis. Table 6 shows that the infill pattern and number of discs have given a significant contribution of 51.60 and 48.29%, respectively, toward the compressive strength. From the result in Table 6, it may also be noted that the *p*-value for the infill pattern and number of discs is significant as the *p*-value is 0.005 and 0.005, respectively. In contrast, the infill density contribution (0.11%) and *p*-value (0.677) are insignificant for the selected DOE.

From Table 7, the infill pattern has played the most vital role in compressive strength as it has been given the first rank. After the infill pattern, the number of discs was ranked second, and the infill density, which contributed the least towards the compressive strength, ranked in third place. Thus, it may be observed that the infill pattern and the number of discs were the most effective input parameters for the 3D printing of PLA.

Figure 6 shows the main effect plot for SN ratios of 3D printed PLA samples. Figure 6 suggests that a honeycomb infill pattern, infill density of 90%, and 6 discs are the recommended settings for the 3D printing of specimens. Figure 7 shows the normal probability plot for the nine samples tested for compressive strength, which indicates that the observations are near the straight line, which signifies that the data was normally distributed. The model was significant as the error component in the normal plot is low, due to which the observations are very near to the straight line. Similarly, the observed trends of the normal plot have been verified by model summary (see Table 8) in which the residual square (R-Square) value of 99.75% is very high; thus, the model seems to be valid.

Table 6. ANOVA table for SN ratios of PLA samples.

Source	DF	Seq SS	Adj SS	Adj MS	F	p	Percentage Contribution
Infill Pattern	2	14.31	14.30	7.15	206.41	0.005	51.60
Infill Density	2	0.03	0.03	0.02	0.48	0.677	0.11
Number of discs	2	13.31	13.31	6.66	192.02	0.005	48.29
Residual Error	2	0.07	0.07	0.04
Total	8	27.72

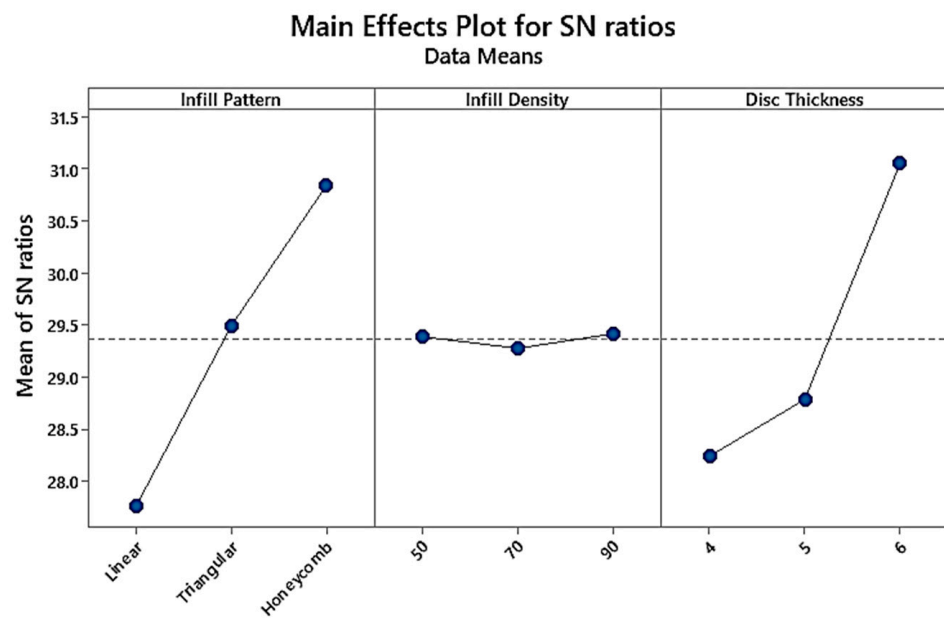
DF: Degree of freedom; Seq SS: Sum of the square; Adj SS: Adjusted sum of the square; Adj MS: Adjusted sum of means; F: Fisher value; p: Probability value.

Table 7. Response Table for SN ratios of PLA samples.

Level	Infill Pattern	Infill Density	Number of Discs
1	27.76	29.39	28.24
2	29.49	29.28	28.79
3	30.84	29.42	31.05
Delta	3.08	0.14	2.81
Rank	1	3	2

Table 8. Model Summary for the PLA samples.

S	R-Sq	R-Sq (Adj)
0.1862	99.75%	99.00%



Signal-to-noise: Larger is better

Figure 6. Main effect plot for SN ratios of PLA samples tested for compressive strength.

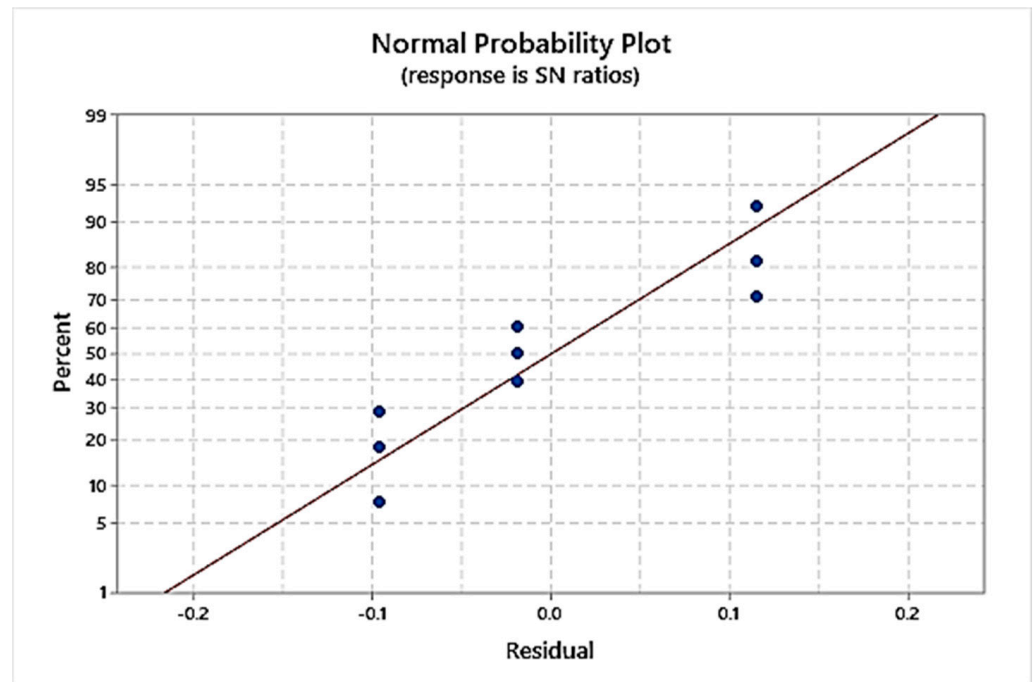


Figure 7. Normal probability plot for PLA samples under compression testing.

4.3. Optimised Setting for FDM Printing

From the model summary and main effect plot, it may be observed that the honeycomb infill pattern, 90% of infill density, and six discs are the recommended settings for 3D printing of PLA samples to maximize the compressive strength. But the suggested setting was not present in the selected DOE. Therefore, theoretical modeling in the ANOVA table was performed to find the maximum suggested compressive strength. Table 9 shows the SN values for the ANOVA table observed by Taguchi 19 OA.

Table 9. SNRA1 values for compressive-tested samples.

Infill Pattern	Infill Density	Number of Disc	Compressive Strength (MPa)	SNRA1
Linear	50	6	29.71	29.46
Linear	70	5	22.40	27.00
Linear	90	4	21.91	26.81
Triangular	50	5	28.38	29.06
Triangular	70	4	25.91	28.27
Triangular	90	6	36.06	31.14
Honeycomb	50	4	30.38	29.65
Honeycomb	70	6	42.47	32.56
Honeycomb	90	5	32.75	30.30

Y_{opt} is the optimized value of peak elongation

$$Z = 29.36 \text{ (See Table 9)}$$

$$Z_{A3} = 30.84 \text{ (See Table 9)}$$

$$Z_{B3} = 29.42 \text{ (See Table 9)}$$

$$Z_{C3} = 31.05 \text{ (See Table 9)}$$

For larger is better case

$$\eta_{opt} = 29.36 + (30.84 - 29.36) + (29.42 - 29.36) + (31.05 - 29.36) \tag{2}$$

$$Z_{opt^2} = \frac{1}{10^{(-\eta_{opt}^2/10)}} \tag{3}$$

$$\eta_{opt} = 32.59\text{dB} \tag{4}$$

$$y_{opt^2} = 1/(10) - 32.59/1$$

$$y_{opt^2} = 1815.16$$

$$y_{opt} = 42.61 \text{ MPa}$$

So, the optimum compressive strength is 42.61 MPa.

The optimized value (42.61 MPa) was observed to be very near to sample 8 (42.47 MPa, see Table 5), in which the setting was a honeycomb pattern, 70% infill density, and 6 number discs. This may be because the infill density was the least effective input parameter for the present study as per the ANOVA results (see Table 6). Thus, the sample 8 input setting for 3D printing and six discs in one sample may be taken as the optimized setting in place of the suggested setting.

4.4. Correlation with the Number of Upper and Lower Layers and Compressive Strength of FDM Printed LOM Joined Samples

This work has considered LOM manufacturing of 3D printed discs of PLA, which requires a different number of discs to be laminated in the single standard sample as per ASTM D790. As per the fixed condition of FDM printing 4 number of lower and upper layers were fabricated for the samples. In the case where there were 4 discs laminated in a single sample, there were a total 32 number of layers (4-upper and 4-lower layers in each disc \times 4 discs = 32 layers). Table 10 shows the number of layers and the compressive strength obtained for the different samples. Using the correlation between the number of layers and compressive strength, it has been observed that as the number of discs increased from four to six, the compressive strength of the specimen increased significantly. This may be due to the reason that the number of solid layers (upper and lower layers) present in the specimen is more in number, each offering individual resisting force and thereby higher overall resistance to the externally applied load.

Figure 8 shows the regression plot for the number of layers and compressive strength of the samples. From Figure 8, it may be observed that the normal plot for the data suggests that the data was normal as the value lies near the normal line. From the residual vs. fit graph, one may find that as the number of layers increased from 4 to 6, the value of compressive strength improved significantly. For 4 discs and 32 layers (rows 3, 5, and 7), the fit value lies near 25 (see residual vs. fit graph in Figure 8), similarly the value of fit for rows 2, 4, and 9 (number of layers: 40) lies near to 30. Whereas, for rows 1, 6, and 8 (number of discs: six, and number of layers: eight), the fit value lies near 35, which was the highest among all the samples. Similar results were observed for the residual vs. observation order graph.

Table 10. Compressive strength Vs. the number of infill layers.

S.No.	Number of Discs	Number of Layers	Compressive Strength
1	6	48	29.71
2	5	40	22.40
3	4	32	21.91
4	5	40	28.38
5	4	32	25.91
6	6	48	36.06
7	4	32	30.38
8	6	48	42.47
9	5	40	32.75

Note: Number of layers = total no. of disc \times 8 (4 upper layers + 4 lower layers); For example: for n = 6 (no. of disc = 6), number of layers = $6 \times 8 = 48$.

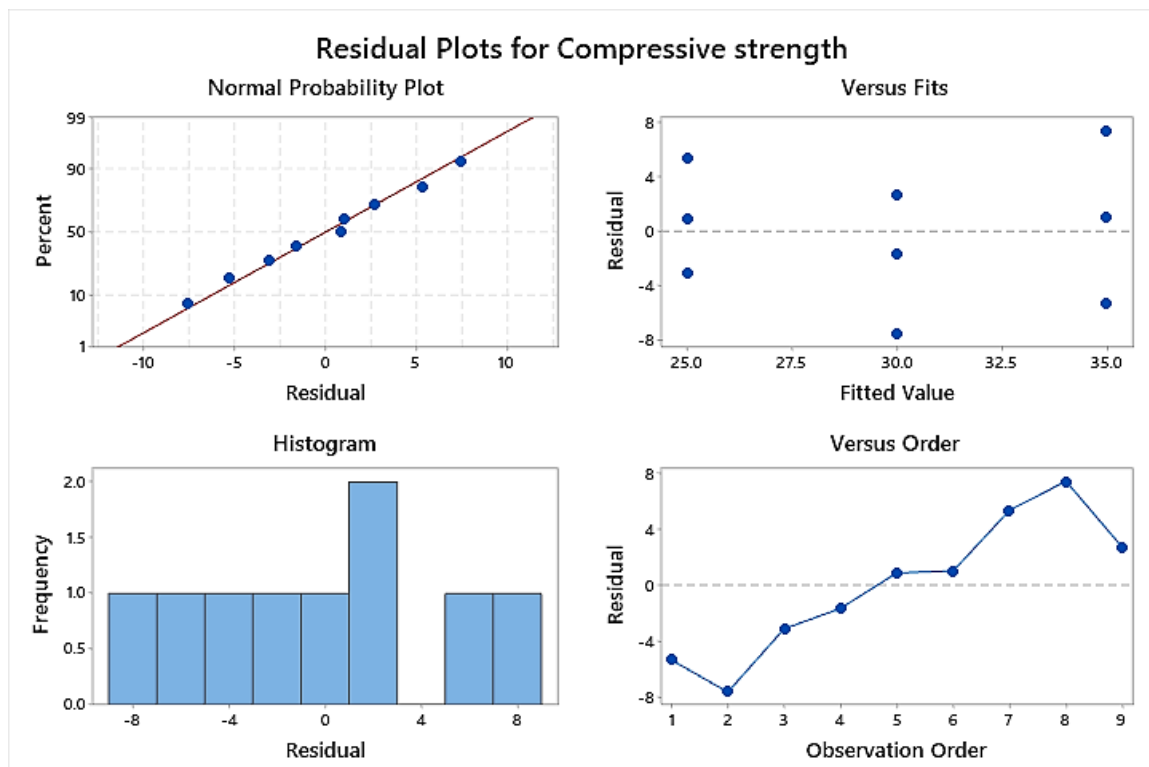


Figure 8. Correlation graph for the number of layers in the sample and compressive strength of the tested samples.

5. Morphological Properties

The mechanical compressive strength of the PLA samples was supported by morphological testing, such as scanning electron microscopy (SEM). Sample 8, with maximum mechanical strength, and sample 3, with least mechanical strength, were analyzed under SEM analysis. Whereas, under the toolmaker microscopic analysis, all samples were tested and analyzed for surface characteristics.

5.1. SEM Analysis

Figure 9 shows the SEM images for samples 3 and 8. The samples were analyzed at $\times 450$ and $\times 900$ magnification, and it may be observed that sample 3 held larger surface irregularities, as evident from Figure 9a,b. The photomicrographic images of the SEM suggest that there are large surface porosities and voids available at the surface. Whereas for sample 8, the surface voids and irregularities were less. Thus, it may be observed that the morphological analysis has supported the mechanical observations. The sizable surface irregularities may be one of the crucial reasons for the poor mechanical performance of sample 3.

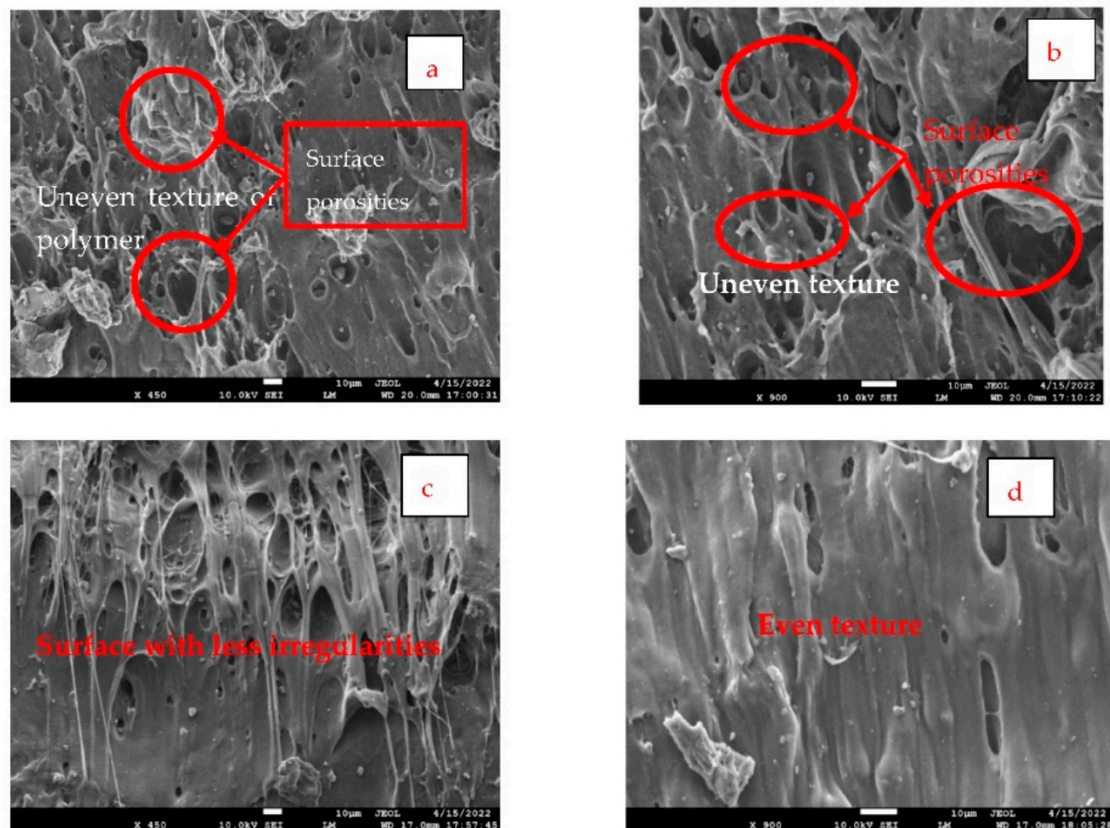


Figure 9. SEM images for sample 3 (a) at $\times 450$ and (b) at $\times 900$ and sample 8 (c) at $\times 450$ and (d) at $\times 900$.

5.2. Tool Maker's Microscopic Image Analysis

The UTM-tested samples were cut from the midplane using a high-speed grinding machine to analyze the different layers under the compression using a Tool Maker's Microscope. From the photomicrographic images of Tool Maker's Microscope, it may be observed in Figure 10 that the samples with six discs (samples 1, 6, and 8) were least disturbed from their axis. Whereas in the case of four discs (samples 3, 5, and 7), the layers were bulged or deflected from the central axis to a significant extent. Thus, it may be noted that fewer discs with high thickness values have resulted in bulging action and thus led to poor mechanical performance. Whereas six discs with less thickness resulted in better compression without any bulging, leading to high mechanical performance.

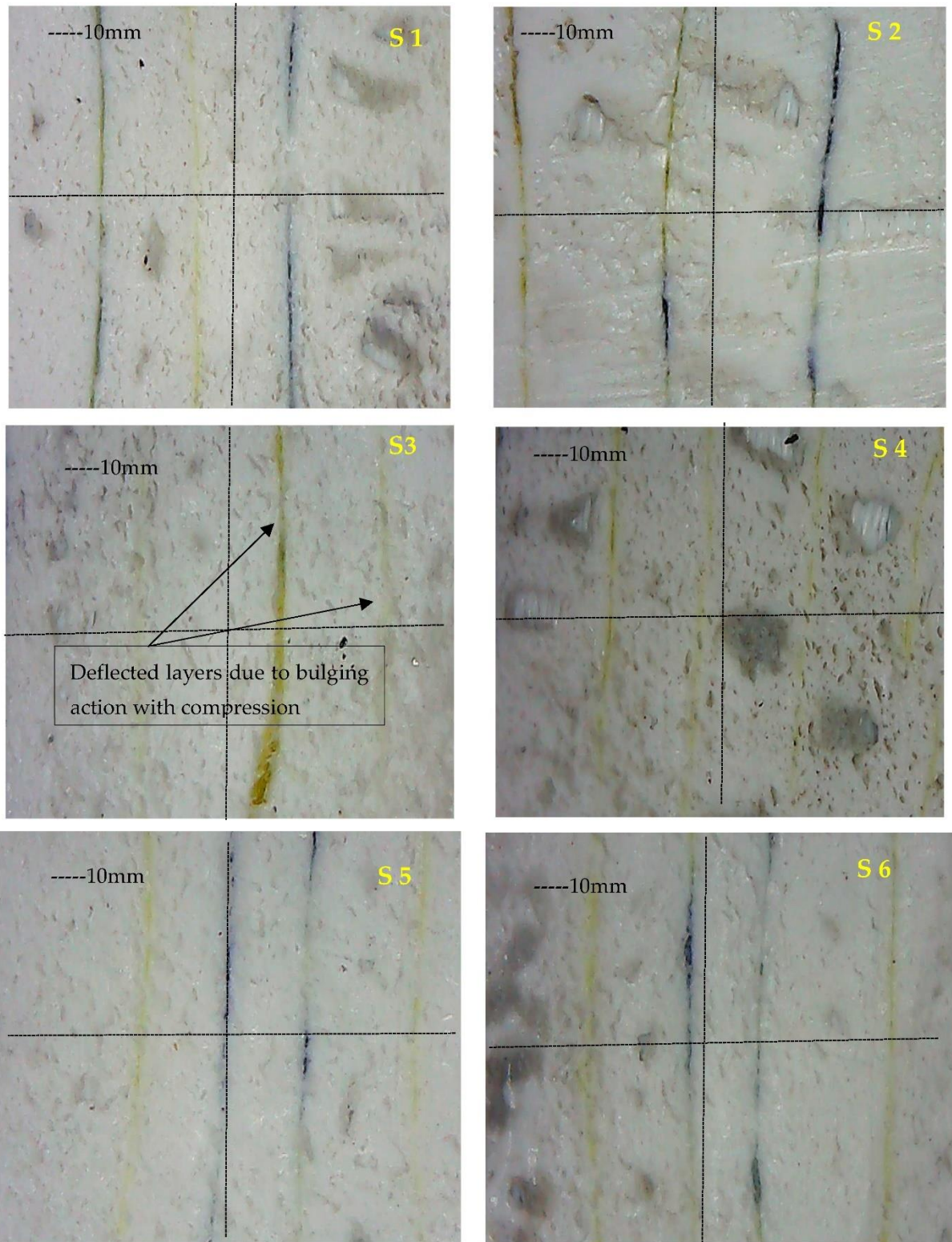


Figure 10. Cont.

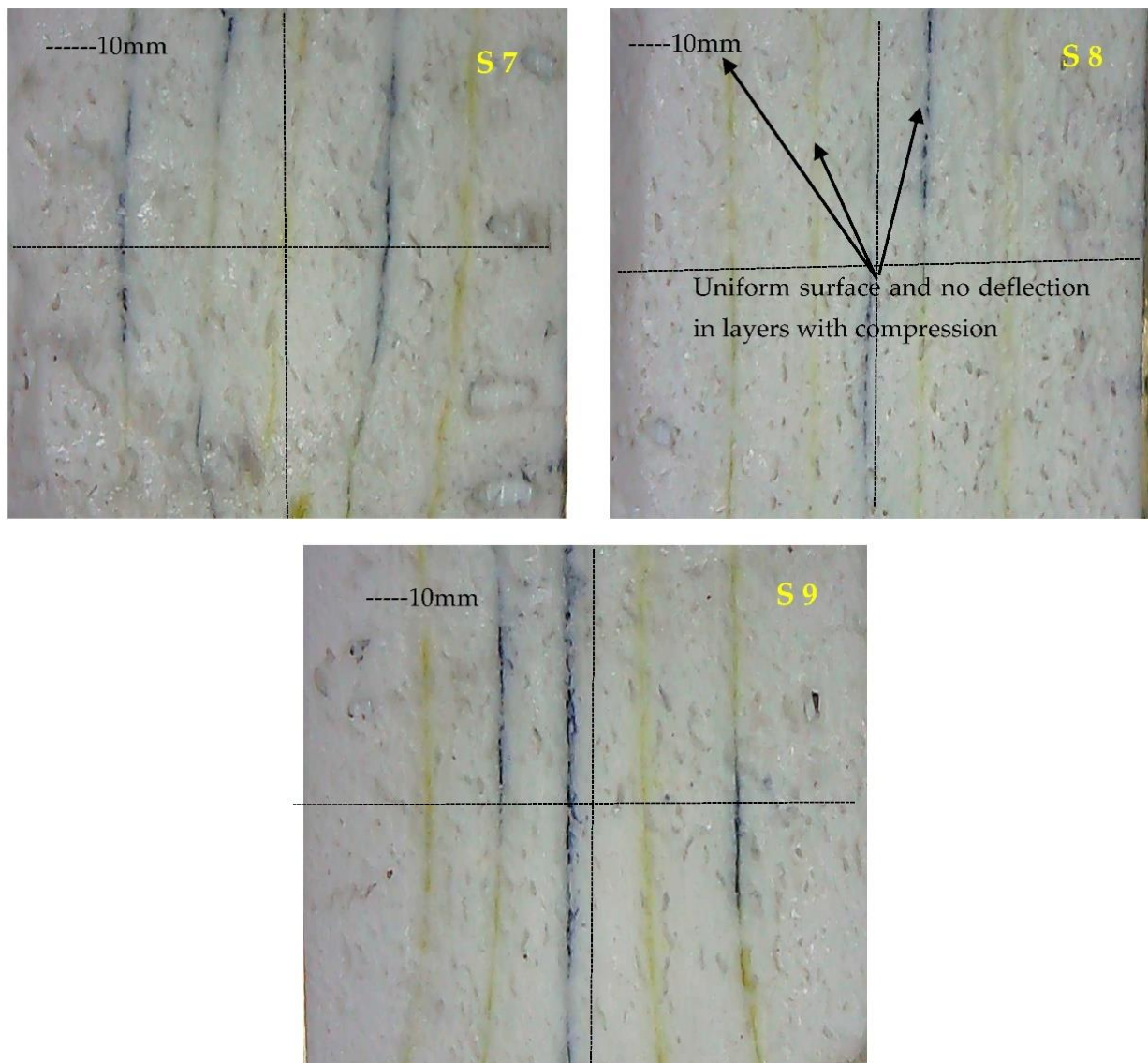


Figure 10. Tool Maker's Microscopic images analysis for compression tested samples of laminated object manufactured 3D printed PLA.

5.3. Surface Roughness Analysis

The photomicrographic images of SEM for sample 3 (Figure 8b) and sample 8 (Figure 8d) were further investigated for surface roughness using the open-source tool for rendering the images. The rendered images' surface roughness analysis suggests that sample 3 held a considerable surface roughness value of 47.26 nm (see Figure 11). Whereas sample 8 has shown the least surface roughness value of 29.42 nm. The low surface roughness value and a smaller number of voids for sample 8 have supported the evaluations for the mechanical behavior of the laminated object manufactured samples.

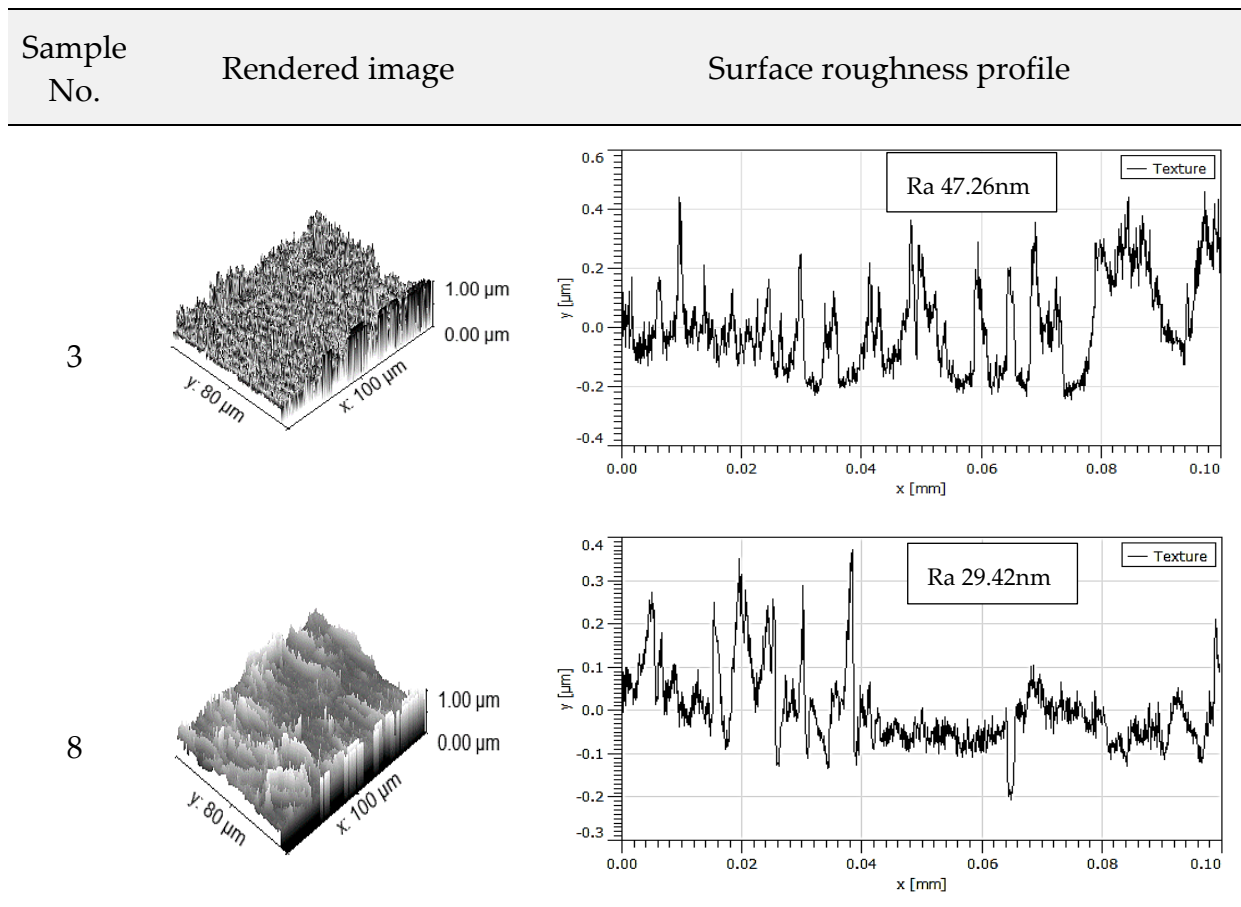


Figure 11. Surface Roughness analysis using Gwydion open software tool.

6. Conclusions

This article investigated the mechanical and morphological properties of poly(lactic acid) specimens using the laminated object manufacturing (LOM) technique. The effect has been experimentally investigated on 3D printed discs joined together to make a laminated test specimen, as per ASTM D695 standard. The specimen with different infill patterns, viz. linear, triangular, and honeycomb structure, 50–90% infill density, and under varying disc thickness ranging from 3.4–5.6 mm, were prepared and tested experimentally. The following significant conclusions have been drawn from the present study:

1. Among the investigated infill patterns, the maximum compressive strength has been seen for the honeycomb infill pattern, followed by the triangular infill and linear infill, respectively. For the laminated object, increasing the number of discs also enhances the compressive strength of all kinds of infill patterns.
2. The maximum compressive strength of 42.47 MPa was attained for the laminated specimen with 70% infill, honeycomb pattern, and disc thickness of 3.4 mm (six discs), whereas the linear infill pattern has shown the least compressive performance of 22.40 MPa. Thus, while using PLA for compressive loading in marine engineering applications, one can choose a honeycomb pattern and six discs with a 70% infill density to have the maximum strength of the samples.
3. An increase in the number of discs has led to higher compressive strength due to reduced bulging action, which has been observed in the microscopic images, whereas the layer bulging was more evident in the laminated objects with a lesser number of discs.
4. From the Taguchi L-9 analysis, the influence of the infill pattern and the number of discs has been observed, contributing 51.60% and 48.29%, respectively, towards the compressive strength, whereas the infill density contribution is insignificant.

The optimum input parameters for laminated object manufacturing for maximum compressive strength have been observed for the Honeycomb infill pattern, 90% infill density, and six discs.

Future Research—The LOM-manufactured samples may have a usage in structural engineering as well as marine engineering applications. The components developed by using multiple components joined in one product may be suitable for marine engineering as the components under ocean water have seen degradation with time. The degraded components can be replaced with new components as per requirements. The LOM technique used in this study may be used in applications where the exposed surfaces of polymers get degraded with time. The degraded portion can be cut off from the surface, and a new FDM printed specimen can be fixed to the sample using epoxy resins.

Author Contributions: Conceptualisation, investigation, methodology, and data curation were performed by S.K., I.S., D.K. and S.S.R.K.; validation, visualization, and formal analysis were performed by S.K., I.S., D.K., M.Y.Y. and S.S.R.K.; resources, writing—original draft preparation, writing—review and editing were performed by S.K., I.S., D.K., M.Y.Y. and S.S.R.K.; supervision was performed by S.K.; project administrations were S.K., M.Y.Y. and S.S.R.K.; funding acquisition was performed by S.S.R.K. All authors have read and agreed to the published version of the manuscript.

Funding: This research received no external funding.

Institutional Review Board Statement: Not applicable.

Informed Consent Statement: Not applicable.

Data Availability Statement: Not applicable.

Acknowledgments: The authors are grateful to CT University for continuous financial, moral, and technical support. The technical assistance provided by CIPET Amritsar and the LPU research lab for the current research work is highly appreciated. The research was partially supported by Universiti Teknologi Malaysia through grant numbers Q.J130000.21A6.00P39 and Q.J130000.3851.19J93. The author acknowledges the support of the Minister of Transport and Construction of the Slovak Republic and the European Union in the transport sector and Information Technology in the frames of the project “Adaptation of 21st-century technologies for non-conventional low-emission vehicles based on composite materials”, Reg. No. NFP313010BXF3 by OPII—VA/DP/2021/9.3-01, as well as the support by the Ministry of Education, Youth, and Sports of the Czech Republic and the European Union (European Structural and Investment Funds Operational Program Research, Development, and Education) in the framework of the project “Modular platform for autonomous chassis of specialized electric vehicles for freight and equipment transportation”, Reg. No. CZ.02.1.01/0.0/0.0/16_025/0007293.

Conflicts of Interest: The authors have no relevant financial or non-financial interests to disclose.

References

1. Upadhyay, R.K.; Mishra, A.K.; Kumar, A. Mechanical Degradation of 3D Printed PLA in Simulated Marine Environment. *Surf. Interfaces* **2020**, *21*, 100778. [[CrossRef](#)]
2. Montalvão, G.R.; Moshrefi-Torbati, M.; Hamilton, A.; Machado, R.; João, A. Behaviour of 3D printed PLA and PLA-PHA in marine environments. *IOP Conf. Ser. Earth Environ. Sci.* **2020**, *424*, 012013. [[CrossRef](#)]
3. Menezes, O.; Roberts, T.; Motta, G.; Patrenos, M.-H.; McCurdy, W.; Alotaibi, A.; Vanderpool, M.; Vaseghi, M.; Beheshti, A.; Davami, K. Performance of Additively Manufactured Polylactic Acid (PLA) in Prolonged Marine Environments. *Polym. Degrad. Stab.* **2022**, *199*, 109903. [[CrossRef](#)]
4. Le Duigou, A.; Davies, P.; Baley, C. Seawater ageing of flax/poly(lactic acid) biocomposites. *Polym. Degrad. Stab.* **2009**, *94*, 1151–1162. [[CrossRef](#)]
5. Mlýnek, J.; Petrů, M.; Martinec, T.; Koloor, S.S.R. Fabrication of High-Quality Polymer Composite Frame by a New Method of Fiber Winding Process. *Polymers* **2020**, *12*, 1037. [[CrossRef](#)]
6. Kumar, S.; Singh, R.; Singh, T.P.; Batish, A. Investigations for mechanical, thermal and magnetic properties of polymeric composite matrix for four-dimensional printing applications. *J. Braz. Soc. Mech. Sci. Eng.* **2020**, *42*, 1–15. [[CrossRef](#)]
7. Wu, D.; Spanou, A.; Diez-Escudero, A.; Persson, C. 3D-printed PLA/HA composite structures as synthetic trabecular bone: A feasibility study using fused deposition modeling. *J. Mech. Behav. Biomed. Mater.* **2020**, *103*, 103608. [[CrossRef](#)]

8. Kolor, S.S.R.; Karimzadeh, A.; Abdullah, M.R.; Petrù, M.; Yidris, N.; Sapuan, S.M.; Tamin, M.N. Linear-Nonlinear Stiffness Responses of Carbon Fiber-Reinforced Polymer Composite Materials and Structures: A Numerical Study. *Polymers* **2021**, *13*, 344. [[CrossRef](#)]
9. Sarabia-Vallejos, M.A.; Rodríguez-Umanzor, F.E.; González-Henríquez, C.M.; Rodríguez-Hernández, J. Innovation in Additive Manufacturing Using Polymers: A Survey on the Technological and Material Developments. *Polymers* **2022**, *14*, 1351. [[CrossRef](#)]
10. Bassoli, E.; Defanti, S.; Tognoli, E.; Vincenzi, N.; Degli Esposti, L. Design for Additive Manufacturing and for Machining in the Automotive Field. *Appl. Sci.* **2021**, *11*, 7559. [[CrossRef](#)]
11. Frohn-Sörensen, P.; Geueke, M.; Engel, B.; Löffler, B.; Bickendorf, P.; Asimi, A.; Bergweiler, G.; Schuh, G. Design for 3D Printed Tools: Mechanical Material Properties for Direct Polymer Additive Tooling. *Polymers* **2022**, *14*, 1694. [[CrossRef](#)] [[PubMed](#)]
12. Rahimian Kolor, S.S.; Karimzadeh, A.; Yidris, N.; Petrù, M.; Ayatollahi, M.R.; Tamin, M.N. An Energy-Based Concept for Yielding of Multidirectional FRP Composite Structures Using a Mesoscale Lamina Damage Model. *Polymers* **2020**, *12*, 157. [[CrossRef](#)] [[PubMed](#)]
13. Khan, M.S.; Abdul-Latif, A.; Kolor, S.S.R.; Petrù, M.; Tamin, M.N. Representative Cell Analysis for Damage-Based Failure Model of Polymer Hexagonal Honeycomb Structure under the Out-of-Plane Loadings. *Polymers* **2020**, *13*, 52. [[CrossRef](#)]
14. Hsissou, R.; Seghiri, R.; Benzekri, Z.; Hilali, M.; Rafik, M.; Elharfi, A. Polymer composite materials: A comprehensive review. *Compos. Struct.* **2021**, *262*, 113640. [[CrossRef](#)]
15. Abdi, B.; Kolor, S.S.R.; Abdullah, M.R.; Amran, A.; Yahya, M.Y. Effect of Strain-Rate on Flexural Behavior of Composite Sandwich Panel. In *Applied Mechanics and Materials*; Trans Tech Publications Ltd.: Fribach, Switzerland, 2012; pp. 766–770. [[CrossRef](#)]
16. Wong, K.J.; Johar, M.; Kolor, S.S.R.; Petrù, M.; Tamin, M.N. Moisture Absorption Effects on Mode II Delamination of Carbon/Epoxy Composites. *Polymers* **2020**, *12*, 2162. [[CrossRef](#)] [[PubMed](#)]
17. Rodrigues, N.; Benning, M.; Ferreira, A.M.; Dixon, L.; Dalgarno, K. Manufacture and characterization of porous PLA scaffolds. *Procedia Cirp* **2016**, *49*, 33–38. [[CrossRef](#)]
18. Song, Y.; Li, Y.; Song, W.; Yee, K.; Lee, K.-Y.; Tagarielli, V. Measurements of the mechanical response of unidirectional 3D-printed PLA. *Mater. Des.* **2017**, *123*, 154–164. [[CrossRef](#)]
19. Serra, T.; Planell, J.; Navarro, M. High-resolution PLA-based composite scaffolds via 3-D printing technology. *Acta Biomater.* **2013**, *9*, 5521–5530. [[CrossRef](#)]
20. Cifuentes, S.; Frutos, E.; Benavente, R.; Lorenzo, V.; González-Carrasco, J. Assessment of mechanical behavior of PLA composites reinforced with Mg micro-particles through depth-sensing indentations analysis. *J. Mech. Behav. Biomed. Mater.* **2017**, *65*, 781–790. [[CrossRef](#)]
21. Abeykoon, C.; Sri-Amphorn, P.; Fernando, A. Optimization of fused deposition modeling parameters for improved PLA and ABS 3D printed structures. *Int. J. Lightweight Mater. Manuf.* **2020**, *3*, 284–297. [[CrossRef](#)]
22. Dave, H.K.; Rajpurohit, S.R.; Patadiya, N.H.; Dave, S.J.; Sharma, K.S.; Thambad, S.S.; Srinivasn, V.P.; Sheth, K.V. Compressive strength of PLA based scaffolds: Effect of layer height, infill density and print speed. *Int. J. Mod. Manuf. Technol.* **2019**, *11*, 21–27.
23. Pilipovic, A.; Raos, P.; Sercer, M. Experimental testing of quality of polymer parts produced by laminated object manufacturing. *Teh. Vjesn.* **2011**, *18*, 253–260.
24. Rubio-López, A.; Olmedo, A.; Díaz-Álvarez, A.; Santiuste, C. Manufacture of compression moulded PLA based biocomposites: A parametric study. *Compos. Struct.* **2015**, *131*, 995–1000. [[CrossRef](#)]
25. Olivier, D.; Travieso-Rodríguez, J.A.; Borros, S.; Reyes, G.; Jerez-Mesa, R. Influence of building orientation on the flexural strength of laminated object manufacturing specimens. *J. Mech. Sci. Technol.* **2017**, *31*, 133–139. [[CrossRef](#)]
26. Senatov, F.S.; Niaza, N.K.; Zadorozhnyy, M.Y.; Maksimkin, A.V.; Kaloshkin, S.D.; Estrin, Y.Z. Mechanical properties and shape memory effect of 3D-printed PLA-based porous scaffolds. *J. Mech. Behav. Biomed. Mater.* **2016**, *57*, 139–148. [[CrossRef](#)]
27. Yadav, P.; Sahai, A.; Sharma, R.S. Strength and Surface Characteristics of FDM-Based 3D Printed PLA Parts for Multiple Infill Design Patterns. *J. Inst. Eng. Ser. C* **2020**, *102*, 197–207. [[CrossRef](#)]
28. Tao, Y.; Yin, Q.; Li, P. An Additive Manufacturing Method Using Large-Scale Wood Inspired by Laminated Object Manufacturing and Plywood Technology. *Polymers* **2020**, *13*, 144. [[CrossRef](#)] [[PubMed](#)]
29. Torre, R.; Brischetto, S.; Dipietro, I.R. Buckling developed in 3D printed PLA cuboidal samples under compression: Analytical, numerical and experimental investigations. *Addit. Manuf.* **2020**, *38*, 101790. [[CrossRef](#)]
30. Singh, S.; Singh, G.; Prakash, C.; Ramakrishna, S.; Lamberti, L.; Pruncu, C.I. 3D printed biodegradable composites: An insight into mechanical properties of PLA/chitosan scaffold. *Polym. Test.* **2020**, *89*, 106722. [[CrossRef](#)]
31. Wang, M.; Jin, G.; He, W.; Nan, F. 3D printing of gun propellants based on laminated object manufacturing. *Mater. Manuf. Process.* **2022**, *37*, 1246–1256. [[CrossRef](#)]
32. Kumar, S.; Singh, R.; Singh, T.; Batish, A. Fused filament fabrication: A comprehensive review. *J. Thermoplast. Compos. Mater.* **2020**. [[CrossRef](#)]
33. Singh, D.; Babbar, A.; Jain, V.; Gupta, D.; Saxena, S.; Dwibedi, V. Synthesis, characterization, and bioactivity investigation of biomimetic biodegradable PLA scaffold fabricated by fused filament fabrication process. *J. Braz. Soc. Mech. Sci. Eng.* **2019**, *41*, 121. [[CrossRef](#)]
34. Singh, R.; Kumar, R.; Singh, M.; Preet, P. On compressive and morphological features of 3D printed almond skin powder reinforced PLA matrix. *Mater. Res. Express* **2019**, *7*, 025311. [[CrossRef](#)]

35. Pavan, M.V.; Balamurugan, K. Compressive test Fractured Surface analysis on PLA-Cu composite filament printed at different FDM conditions. *IOP Conf. Ser. Mater. Sci. Eng.* **2020**, *988*, 012019. [[CrossRef](#)]
36. Haaparanta, A.-M.; Järvinen, E.; Cengiz, I.F.; Ellä, V.; Kokkonen, H.T.; Kiviranta, I.; Kellomäki, M. Preparation and characterization of collagen/PLA, chitosan/PLA, and collagen/chitosan/PLA hybrid scaffolds for cartilage tissue engineering. *J. Mater. Sci. Mater. Med.* **2013**, *25*, 1129–1136. [[CrossRef](#)]
37. Kumar, S.; Singh, R.; Singh, T.; Batish, A. On investigations of thermal conductivity, circumferential compressive strength, and surface characterization of 3D-printed hybrid blended magnetostrictive PLA composite. *J. Thermoplast. Compos. Mater.* **2020**, *35*, 631–650. [[CrossRef](#)]
38. Scaffaro, R.; Lopresti, F.; Botta, L.; Rigogliuso, S.; Ghersi, G. Preparation of three-layered porous PLA/PEG scaffold: Relationship between morphology, mechanical behavior and cell permeability. *J. Mech. Behav. Biomed. Mater.* **2016**, *54*, 8–20. [[CrossRef](#)]
39. Parandoush, P.; Li, X.; Chang, B.; Sorensen, C.M.; Shi, J.; Liu, Y.; Lin, D. Additive manufacturing of continuous carbon fiber reinforced epoxy composite with graphene enhanced interlayer bond toward ultra-high mechanical properties. *Polym. Compos.* **2021**, *43*, 934–945. [[CrossRef](#)]
40. Mohammed, J.S. Applications of 3D printing technologies in oceanography. *Methods Oceanogr.* **2016**, *17*, 97–117. [[CrossRef](#)]
41. Palaniyappan, S.; Veeman, D.; Kumar, S.N.; Surendhar, G.J.; Natrayan, L. Effect of printing characteristics for the incorporation of hexagonal-shaped lattice structure on the PLA polymeric material. *J. Thermoplast. Compos. Mater.* **2022**. [[CrossRef](#)]
42. Çamlı, S.; Neşer, G.; Sözen, A. Polylactic Acid (pla) and Wood Composite as a Sustainable Material Alternative in Additive Boat Manufacturing and Its Degradation in Marine Environment. In Proceedings of the 25th Symposium on Theory and Practice of Shipbuilding, Malinska, Croatia, 7–10 September 2022.
43. Kumar, S.; Singh, I.; RKolloor, S.S.; Kumar, D.; Yahya, M.Y. On Laminated Object Manufactured FDM-Printed ABS/TPU Multimaterial Specimens: An Insight into Mechanical and Morphological Characteristics. *Polymers* **2022**, *14*, 4066. [[CrossRef](#)]
44. Almonti, D.; Baiocco, G.; Mingione, E.; Ucciardello, N. Evaluation of the effects of the metal foams geometrical features on thermal and fluid-dynamical behavior in forced convection. *Int. J. Adv. Manuf. Technol.* **2020**, *111*, 1157–1172. [[CrossRef](#)]
45. Almonti, D.; Mingione, E.; Tagliaferri, V.; Ucciardello, N. Design and analysis of compound structures integrated with bio-based phase change materials and lattices obtained through additive manufacturing. *Int. J. Adv. Manuf. Technol.* **2021**, *119*, 149–161. [[CrossRef](#)]
46. Mekonnen, B.G.; Bright, G.; Walker, A. A Study on State of the Art Technology of Laminated Object Manufacturing (LOM). In *CAD/CAM, Robotics and Factories of the Future 2016*; Springer: New Delhi, India, 2016; pp. 207–216. [[CrossRef](#)]
47. Ahn, H.; Lee, D.; Ji, W.; Lee, W.; Cho, H. Development of Method for Manufacturing Freeform EPS Forms Using Sloped-LOM Type 3D Printer. *J. Korea Inst. Build. Constr.* **2020**, *20*, 171–181.
48. Ligon, S.C.; Liska, R.; Stampfl, J.; Gurr, M.; Mülhaupt, R. Polymers for 3D Printing and Customized Additive Manufacturing. *Chem. Rev.* **2017**, *117*, 10212–10290. [[CrossRef](#)]
49. Pérez-Fonseca, A.A.; Martín Del Campo, A.S.; Robledo-Ortíz, J.R.; González-López, M.E. Compatibilization strategies for PLA biocomposites: A comparative study between extrusion-injection and dry blending-compression molding. *Compos. Interfaces* **2022**, *29*, 274–292. [[CrossRef](#)]